Biophysical Letter

Molecular Order of Arterial Collagen Using Circular Polarization Second-Harmonic Generation Imaging

Raphaël Turcotte,[1,2] Jeffrey M. Mattson,[3] Juwell W. Wu,[1] Yanhang Zhang,[2,3] and Charles P. Lin[1,*]
[1]Wellman Center for Photomedicine and Center for System Biology, Massachusetts General Hospital, Harvard Medical School, Boston, Massachusetts; [2]Department of Biomedical Engineering and [3]Department of Mechanical Engineering, Boston University, Boston, Massachusetts

ABSTRACT Second-harmonic generation (SHG) originates from the interaction between upconverted fields from individual scatterers. This renders SHG microscopy highly sensitive to molecular distribution. Here, we aim to take advantage of the difference in SHG between aligned and partially aligned molecules to probe the degree of molecular order during biomechanical testing, independently of the absolute orientation of the scattering molecules. Toward this goal, we implemented a circular polarization SHG imaging approach and used it to quantify the intensity change associated with collagen fibers straightening in the arterial wall during mechanical stretching. We were able to observe the delayed alignment of collagen fibers during mechanical loading, thus demonstrating a simple method to characterize molecular distribution using intensity information alone.

Received for publication 16 July 2015 and in final form 28 December 2015.

*Correspondence: lin@helix.mgh.harvard.edu

Many cardiovascular diseases have been linked to altered mechanical functions in arteries (1). Understanding their pathomechanics and developing treatments require a deeper understanding of the interplay between the mechanical properties at the tissue level and the extracellular matrix (ECM) organization at the microstructural level, a multiscale problem. Collagen fibers are one of the principal ECM components involved in arterial wall mechanics and can be imaged label-free with second-harmonic microscopy (2). Extracting structural information, however, involves time consuming analysis of multiple second-harmonic images (3). Recently, circularly polarized nonlinear optics was shown to have the ability to quantify molecular symmetry after the acquisition of a minimal number of images using exclusively intensity information (4). We therefore set out to explore if circularly polarized illumination can be exploited to quantify the molecular alignment in arterial collagen with a single image during mechanical loading.

Second-harmonic scattering of a single molecule is a coherent parametric process during which the energy of two incident photons at frequency ν_i is redirected to a single photon at frequency $2\nu_i$. The coherence of second-harmonic scattering implies that the generated light depends on both the amplitude and the phase of the incident field. Thus, when multiple scatterers are present, the second-harmonic fields will interfere together and generate an often complex radiation pattern. This is second-harmonic generation (SHG). For a given distribution, the SHG signal is maximal when all scattering molecules possess the same orientation (Fig. 1 *a*) (5,6). In biomedical applications, observing a perfect alignment of molecules is unlikely. Even highly organized structures, such as cell membranes or collagen fibrils, are likely to have some angular distribution in their dipole orientation (Fig. 1 *b*), resulting in weaker SHG signal.

The above discussion implies that changes in molecular organization on the scale of the phase coherence length can be monitored by intensity measurements alone. The dynamics of dye reorientation within lipid bilayers was previously followed using the variation in second-harmonic intensity relative to two-photon excited fluorescence (TPEF) (5). The relative gain or loss in SHG signal was quantified using: $\Theta_2 = I_{SHG}/I_{SHG}^{max}$. During mechanical stretching of arterial tissue, collagen fibers are known to straighten (3). This alignment of collagen is expected to lead to changes in the molecular orientation, hence changes in I_{SHG}. Here, our goal is to demonstrate that such changes in I_{SHG} can be detected during the deformation of arteries, thus enabling the characterization of fiber engagement with simple normalized intensity measurements.

Second-harmonic imaging was performed on a custom laser scanning microscope described in detail elsewhere (7). Collagen was imaged at 30 frames/s with 25 mW from a mode-locked Ti:sapph laser at 800 nm (Maitai-HP, Spectra-Physics, Santa Clara, CA) through a 60X objective

Editor: Andrew McCulloch

http://dx.doi.org/10.1016/j.bpj.2015.12.030

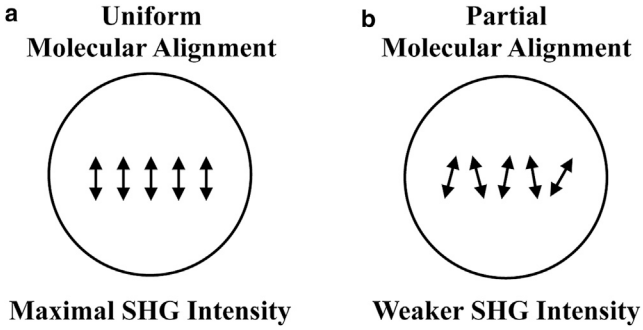

FIGURE 1 The intensity originating from second-harmonic fields depends on molecular alignment for any incident polarization state. (*a*) The SHG signal is maximal if all molecules (↕) are aligned. (*b*) Partial alignment of molecules results in weaker SHG signal.

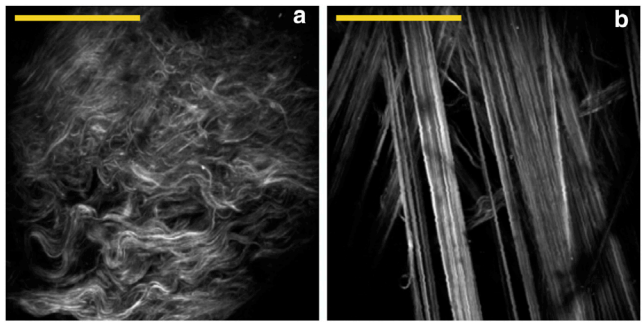

FIGURE 2 Evaluation of the engagement of collagen fibers during mechanical loading by systematic random imaging. Second-harmonic images of adventitial collagen at strains of (*a*) 0% and (*b*) 40% showing fiber straightening (scale bar, 180 μm, 30 frames average).

lens (NA1.0 W, LUMPlanN, Olympus, Waltham, MA) (3). Circular polarization of the illumination light was obtained by placing a quarter-wave plate just before the objective. The polarization was verified to be maintained at the focus by rotating mouse tail tendons ($\Delta I_{SHG} < 5\%$) and imaging spherical cells (NALM6, a leukemic cell line) labeled with Di-8-ANEPPS ($\Delta I_{TPEF} < 3\%$, n=60) (8). Imaging was performed on the adventitia, the external portion of arterial walls, of excised pig aorta down to a depth of 60 μm. Arteries ($n = 6$) were placed on a stretching device according to standard testing procedures (3).

To test for changes in second-harmonic intensity, we imaged freshly excised aorta under equal biaxial strains from 0 to 40% with 5% increments at multiple random locations (nine regions over a 1 cm^2 area). The strain was always equal biaxial (i.e., the same in the longitudinal and circumferential direction) and defined as $\tau = (L_i - L_0)/L_0$, where L_0 is the unstretched tissue length and L_i is the length at strain i. Using this approach, together with a manual measurement of fiber waviness or an automated fractal analysis (3), we previously reported a delayed realignment of adventitial collagen. Collagen fibers are highly wavy at 0% strain (Fig. 2 *a*) but are completely straight at 40% (Fig. 2 *b*). The adventitial collagen undergoes large structural changes that can be characterized with direct biophysical measurements, making it an ideal site to validate new experimental strategies. Analyses were performed on maximum intensity projection images of axial stacks over 110 × 110 μm regions. For image intensity measurements, a fixed threshold of 10 on a 8-bit scale was used to isolate all fibers, and the average image intensity was calculated using only pixels where fibers were present. This procedure ensured that the amount of fibers did not bias the intensity evaluation. Fig. 3 *a* shows that the intensity was constant between 0 and 20% strain. The increase in intensity >20% strain revealed the same delayed fiber recruitment, as described previously, without the need to perform tedious manual measurements or employ advanced image analysis methods.

Tissue stretching in the longitudinal and circumferential axes also impacts the radial thickness (Fig. S1 in the Supporting Material). Therefore, the absolute depth of objects could be altered by volumetric deformation (i.e., collagen fibers might become more superficial). To verify if the increased I_{SH} was due to volumetric deformation, I_{SH} was compared to I_{TPEF}, a fully incoherent process. For this purpose, arteries were incubated at 4°C overnight in a PBS solution containing fluorescein, which possesses a strong TPEF cross section. After imaging, the SHG and TPEF intensities were evaluated in individual collagen fiber bundles at strains of 0, 20, and 40% by cropping 18 × 18 μm regions. The SHG intensity from each region was then normalized to the TPEF signal from fluorescein. A significant increase in the SHG/TPEF ratio was observed at 40% strain, but not 20% (Fig. 3 *b*). This indicates that the increase in SHG intensity is associated with changes in molecular organization and not volumetric deformation.

The information on the molecular distribution within a nonlinear excitation volume can be obtained using polarimetric second-harmonic imaging (9,10). By acquiring multiple images with a linearly polarized illumination with different orientation, the nonlinear susceptibility tensor $\chi^{(2)}$ can be probed ($\rho_1 = \chi_{zzz}/\chi_{zxx}$ and $\rho_2 = \chi_{xzx}/\chi_{zxx}$) using:

$$I_{SHG}^{Lin}(2\nu_i, \theta) = I_0\left[(\rho_2 sin(2\theta))^2 + \left(sin^2(\theta) + \rho_1 cos^2(\theta)\right)^2\right], \quad (1)$$

where $I_0 = c\epsilon_0^2\chi_{zxx}^2|E(\nu_i)|^4$ (see Supporting Material for the derivation of Eq. 1) (11–13). $\chi^{(2)}$ is a bulk property and dependent on molecular arrangement. It is usually assumed that the susceptibility of individual molecules remains unchanged. Effective changes in susceptibility are instead attributed to an increase or decrease molecular order. This method was previously applied to mechanical testing on tendons and shown to be sensitive to collagen fiber straightening and alignment (10,14). To link our relative intensity measurement to polarimetric imaging, we derived an

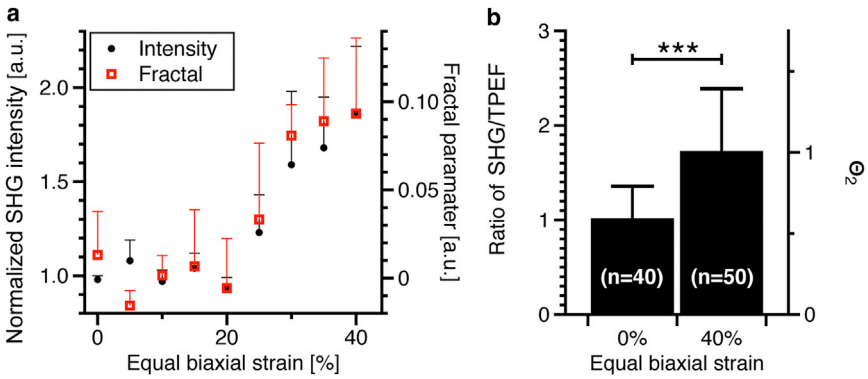

FIGURE 3 Collagen fibers straightening. (*a*) The fractal analysis from Chow et al. (3) and the normalized intensity measurement both show delayed collagen fiber realignment ($n = 6$). (*b*) The ratio between SHG and TPEF intensity in collagen fiber bundles stained with fluorescein was evaluated at strains of 0 and 40%. Mann-Whitney U-test with *** $p = 3.6 \times 10^{-8}$.

expression equivalent to Eq. 1 for circularly incident illumination (see Supporting Material):

$$I_{SHG}^{Cir}(2\nu_i) = \frac{I_0}{4}\left[4\rho_2^2 + (\rho_1 - 1)^2\right]. \quad (2)$$

When a strain of 40% is applied on an artery, collagen fibers are fully aligned, and it can be assumed that the second-harmonic signal is maximal. The relative decrease in intensity at lower strain can therefore be expressed as:

$$\Theta_2(\tau) = \frac{I_{SHG}^{Cir}(2\nu_i, \tau)}{I_{SHG}^{Cir}(2\nu_i, 40\%)} \quad (3)$$

$$= \frac{4\rho_2^2(\tau) + [\rho_1(\tau) - 1]^2}{4\rho_2^2(40\%) + [\rho_1(40\%) - 1]^2}. \quad (4)$$

Polarimetric second-harmonic imaging has the advantage of providing absolute values for ρ_i, but the imaging speed is limited by the need to acquire multiple images at a single location and to control the incident light polarization (15). In contrast, our intensity measurement with circular polarization provides relative values at greater imaging speed and experimental simplicity, eliminating the need to acquire multiple images at different polarizations. It should be possible to implement the method for intravital imaging applications of rapidly deforming tissue, such as arteries and contracting muscles (16).

Our method relies critically on the circularly polarized excitation beam. Because this polarization will not be maintained after propagation in tissue, only the most superficial layer of collagen was analyzed in this work. This was accomplished by taking the maximum intensity projection of the image stack. More sophisticated methods requiring full polarimetry will be needed to account for altered polarization due to birefringence and diattenuation when imaging deeper into tissue (10,17).

In summary, we demonstrate a method for characterizing mechanical functions of arterial collagen at the molecular level with single SHG images acquired with circularly polarized light. During tissue stretching, we observed an increase in second-harmonic intensity, attributable to increased molecular order and directly related to changes in the nonlinear susceptibility tensor of the material (Eq. 4). The SHG intensity with circularly polarized light is not sensitive to the absolute orientation of the scatterers, thus enabling characterization of their relative degree of order with a single image per tissue state. Finally, we believe that the simplicity of our approach will enable characterization of tissue properties in several biomedical applications, especially when fast image acquisition is required.

SUPPORTING MATERIAL

Supporting Mathematical Derivation and one figure are available at http://www.biophysj.org/biophysj/supplemental/S0006-3495(16)00002-3.

AUTHOR CONTRIBUTIONS

R.T., J.M.M., and J.W.W. performed the experiments. R.T., Y.Z. and C.L.P. wrote the manuscript and designed the experiments.

ACKNOWLEDGMENTS

We thank Dr. Ming-Jay Chow for his help with mechanical testing.

This work is supported in part by NIH grant Nos. U01 HL099997 (to C.L.P.) and NIH R01 HL098028 (to Y.Z.). R.T. was supported by a FRQNT PhD Fellowship and a Wellman Center for Photomedicine Graduate Student Fellowship.

REFERENCES

1. Safar, M. E., M. F. O'Rourke, and E. D. Frohlich. 2014. Blood Pressure and Arterial Wall Mechanics in Cardiovascular Diseases. Springer-Verlag, London.
2. Zoumi, A., X. Lu, …, B. J. Tromberg. 2004. Imaging coronary artery microstructure using second-harmonic and two-photon fluorescence microscopy. *Biophys. J.* 87:2778–2786.
3. Chow, M.-J., R. Turcotte, …, Y. Zhang. 2014. Arterial extracellular matrix: a mechanobiological study of the contributions and interactions of elastin and collagen. *Biophys. J.* 106:2684–2692.

4. Duboisset, J., H. Rigneault, and S. Brasselet. 2014. Filtering of matter symmetry properties by circularly polarized nonlinear optics. *Phys. Rev. A.* 90:063827.
5. Moreaux, L., O. Sandre, …, J. Mertz. 2001. Coherent scattering in multi-harmonic light microscopy. *Biophys. J.* 80:1568–1574.
6. Mertz, J. 2009. Introduction to Optical Microscopy. Roberts and Company Publishers, Greenwood Village, CO.
7. Veilleux, I., J. A. Spencer, …, C. P. Lin. 2008. In vivo cell tracking with video rate multimodality laser scanning microscopy. *IEEE J. Sel. Top. Quant.* 14:10–18.
8. Chen, X., O. Nadiarynkh, …, P. J. Campagnola. 2012. Second harmonic generation microscopy for quantitative analysis of collagen fibrillar structure. *Nat. Protoc.* 7:654–669.
9. Campagnola, P. J., and C.-Y. Dong. 2011. Second harmonic generation microscopy: principles and applications to disease diagnosis. *Laser Photonics Rev.* 5:12–26.
10. Gusachenko, I., V. Tran, …, M. C. Schanne-Klein. 2012. Polarization-resolved second-harmonic generation in tendon upon mechanical stretching. *Biophys. J.* 102:2220–2229.
11. Butcher, P. N., and D. Cotter. 1990. The Elements of Nonlinear Optics. Cambridge University Press, London.
12. Plotnikov, S. V., A. C. Millard, …, W. A. Mohler. 2006. Characterization of the myosin-based source for second-harmonic generation from muscle sarcomeres. *Biophys. J.* 90:693–703.
13. Chen, W. L., T. H. Li, …, C. Y. Dong. 2009. Second harmonic generation χ tensor microscopy for tissue imaging. *Appl. Phys. Lett.* 94:2007–2010.
14. Goulam Houssen, Y., I. Gusachenko, …, J. M. Allain. 2011. Monitoring micrometer-scale collagen organization in rat-tail tendon upon mechanical strain using second harmonic microscopy. *J. Biomech.* 44:2047–2052.
15. Bélanger, E., R. Turcotte, …, D. C. Côté. 2015. Maintaining polarization in polarimetric multiphoton microscopy. *J. Biophotonics.* 8:884–888.
16. Psilodimitrakopoulos, S., P. Loza-Alvarez, and D. Artigas. 2014. Fast monitoring of in-vivo conformational changes in myosin using single scan polarization-SHG microscopy. *Biomed. Opt. Express.* 5:4362–4373.
17. Gusachenko, I., G. Latour, and M. C. Schanne-Klein. 2010. Polarization-resolved Second Harmonic microscopy in anisotropic thick tissues. *Opt. Express.* 18:19339–19352.

Biophysical Journal

Supporting Material

Molecular Order of Arterial Collagen Using Circular Polarization Second-Harmonic Generation Imaging

Raphaël Turcotte,[1,2] Jeffrey M. Mattson,[3] Juwell W. Wu,[1] Yanhang Zhang,[2,3] and Charles P. Lin[1,*]

[1]Wellman Center for Photomedicine and Center for System Biology, Massachusetts General Hospital, Harvard Medical School, Boston, Massachusetts; and [2]Department of Biomedical Engineering and [3]Department of Mechanical Engineering, Boston University, Boston, Massachusetts

*Correspondence: lin@helix.mgh.harvard.edu

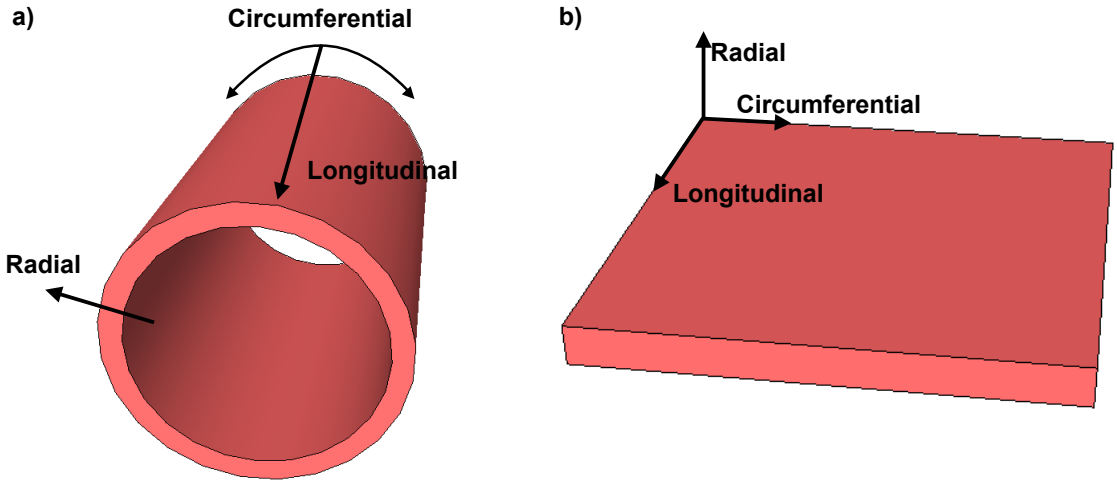

Supporting Fig 1 Diagram showing axial, circumferential, and radial directions in a) intact and b) cut-open arteries. Arteries are cut-open along the longitudinal direction.

Derivation of SHG Polarizability for collagen fibers

The general form of the second order polarizability is:[1]

$$\mathbf{P}^{(2)}_{\text{SHG}} = \epsilon_0 \chi^{(2)} \mathbf{E}, \tag{1}$$

where $\chi^{(2)}$ is the third rank tensor for the second order nonlinear susceptibility

$$\chi^{(2)} = \begin{bmatrix} \chi_{xxx} & \chi_{xyy} & \chi_{xzz} & \chi_{xxy} & \chi_{xxz} & \chi_{xyx} & \chi_{xzx} & \chi_{xyz} & \chi_{xzy} \\ \chi_{yxx} & \chi_{yyy} & \chi_{yzz} & \chi_{yxy} & \chi_{yxz} & \chi_{yyx} & \chi_{yzx} & \chi_{yyz} & \chi_{yzy} \\ \chi_{zxx} & \chi_{zyy} & \chi_{zzz} & \chi_{zxy} & \chi_{zxz} & \chi_{zyx} & \chi_{zzx} & \chi_{zyz} & \chi_{zzy} \end{bmatrix}, \tag{2}$$

and $\mathbf{E}$ is the general incident fields vector:

$$\mathbf{E} = \begin{bmatrix} E_x(\omega)E_x(\omega) \\ E_y(\omega)E_y(\omega) \\ E_z(\omega)E_z(\omega) \\ E_x(\omega)E_y(\omega) \\ E_x(\omega)E_z(\omega) \\ E_y(\omega)E_x(\omega) \\ E_z(\omega)E_x(\omega) \\ E_y(\omega)E_z(\omega) \\ E_z(\omega)E_y(\omega) \end{bmatrix}. \tag{3}$$

With c being a proportionality constant, the second-order polarizability is linked to the intensity by:

$$I = c[P^{(2)}_x P^{(2)*}_x + P^{(2)}_y P^{(2)*}_y + P^{(2)}_z P^{(2)*}_z], \tag{4}$$

Several symmetry arguments can be made to simplified the $\chi^{(2)}$ tensor. These arguments depend on the properties of the nonlinear process, but also on sample. For SHG in collagen fibers, hexagonal symmetry applies and the only non-zero elements are d_{33}, d_{31}, d_{15}, and d_{14}.[1] d_{is} is defined as χ_{ijk} with $i, j, k = \{x, y, z\}$ and $s = 1, 2, 3, 4, 5, 6$ for $xx, yy, zz, \{yz, zy\}, \{xz, zx\}$, and $\{xy, yx\}$ respectively. Eq. (2) can thus be written as:

$$\chi^{(2)} = \begin{bmatrix} 0 & 0 & 0 & 0 & a & 0 & a & b & b \\ 0 & 0 & 0 & 0 & -b & 0 & -b & a & a \\ m & m & n & 0 & 0 & 0 & 0 & 0 & 0 \end{bmatrix}, \tag{5}$$

where $a = d_{15}$, $b = d_{14}$, $m = d_{31}$, and $n = d_{33}$.

Cylindrical symmetry is also often considered.[2] Assuming cylindrical symmetry ($b = 0$ and $a = m$) is equivalent to assuming Kleinman symmetry. The experimental a/m ratio is not exactly 1 and both terms are usually kept.[3] This allows to express Eq. (5) as:

$$\chi^{(2)} = \begin{bmatrix} 0 & 0 & 0 & 0 & a & 0 & a & 0 & 0 \\ 0 & 0 & 0 & 0 & 0 & 0 & 0 & a & a \\ m & m & n & 0 & 0 & 0 & 0 & 0 & 0 \end{bmatrix}. \tag{6}$$

Assuming y-axis propagation of excitation fields ($E_y = 0$), Eq. (1) can be written as:

$$\begin{bmatrix} P_x^{(2)}(2\omega) \\ P_y^{(2)}(2\omega) \\ P_z^{(2)}(2\omega) \end{bmatrix} = \epsilon_0 \begin{bmatrix} 0 & 0 & 0 & 0 & a & 0 & a & 0 & 0 \\ 0 & 0 & 0 & 0 & 0 & 0 & 0 & a & a \\ m & m & n & 0 & 0 & 0 & 0 & 0 & 0 \end{bmatrix} \begin{bmatrix} E_x(\omega)E_x(\omega) \\ 0 \\ E_z(\omega)E_z(\omega) \\ 0 \\ E_x(\omega)E_z(\omega) \\ 0 \\ E_z(\omega)E_x(\omega) \\ 0 \\ 0 \end{bmatrix}, \text{ or} \tag{7}$$

$$\begin{bmatrix} P_x^{(2)}(2\omega) \\ P_y^{(2)}(2\omega) \\ P_z^{(2)}(2\omega) \end{bmatrix} = \epsilon_0 \begin{bmatrix} \chi_{xzx}E_x(\omega)E_z(\omega) + \chi_{xzx}E_z(\omega)E_x(\omega) \\ 0 \\ \chi_{zxx}E_x(\omega)E_x(\omega) + \chi_{zzz}E_z(\omega)E_z(\omega) \end{bmatrix}. \tag{8}$$

Eq. (8) is valid only when hexagonal and cylindrical symmetries apply and can be used for any incident polarization state.

Intensity for linearly polarized light

The electric field for linearly polarization light can be expressed in terms of the Jones vector:

$$\mathbf{E} = |\mathbf{E}| Re\{|\psi\rangle exp[i(ky)]\}, \text{ where} \tag{9}$$

$$|\psi\rangle = \begin{bmatrix} cos(\theta) \\ sin(\theta) \end{bmatrix} exp[i\alpha]. \tag{10}$$

The electric field can therefore be decomposed as $E_z(\omega) = |E(\omega)|cos(\theta)$ and $E_x(\omega) = |E(\omega)|sin(\theta)$. For linearly polarized light, Eq. (8) can thus be expressed as:

$$\begin{bmatrix} P_x^{(2)}(2\omega) \\ P_y^{(2)}(2\omega) \\ P_z^{(2)}(2\omega) \end{bmatrix} = \epsilon_0 \begin{bmatrix} \chi_{xzx}|E(\omega)||E(\omega)|sin(\theta)cos(\theta)+\chi_{xzx}|E(\omega)||E(\omega)|sin(\theta)cos(\theta) \\ 0 \\ \chi_{zxx}|E(\omega)||E(\omega)|sin(\theta)sin(\theta)+\chi_{zzz}|E(\omega)||E(\omega)|cos(\theta)cos(\theta) \end{bmatrix}, \tag{11}$$

$$\begin{bmatrix} P_x^{(2)}(2\omega) \\ P_y^{(2)}(2\omega) \\ P_z^{(2)}(2\omega) \end{bmatrix} = \epsilon_0 |E(\omega)|^2 \begin{bmatrix} 2\chi_{xzx}sin(\theta)cos(\theta) \\ 0 \\ \chi_{zxx}sin^2(\theta)+\chi_{zzz}cos^2(\theta) \end{bmatrix}, \text{ or} \tag{12}$$

$$\begin{bmatrix} P_x^{(2)}(2\omega) \\ P_y^{(2)}(2\omega) \\ P_z^{(2)}(2\omega) \end{bmatrix} = \epsilon_0 |E(\omega)|^2 \begin{bmatrix} \chi_{xzx}sin(2\theta) \\ 0 \\ \chi_{zxx}sin^2(\theta)+\chi_{zzz}cos^2(\theta) \end{bmatrix}. \tag{13}$$

Using Eq. (13) in Eq. (4), we obtain the commonly used expression for the SHG intensity in polarimetric measurements:[3]

$$I_{SHG}^{Lin}(2\omega, \theta) = c\epsilon_0^2 |E(\omega)|^4 \left[(\chi_{xzx}sin(2\theta))^2 + (\chi_{zxx}sin^2(\theta) + \chi_{zzz}cos^2(\theta))^2 \right]. \tag{14}$$

A standard notation for Eq. (14) uses $\rho_1 = \chi_{zzz}/\chi_{zxx}$ and $\rho_2 = \chi_{xzx}/\chi_{zxx}$:[3]

$$I_{SHG}^{Lin}(2\omega, \theta) = c\epsilon_0^2 \chi_{zxx}^2 |E(\omega)|^4 \left[(\rho_2 sin(2\theta))^2 + (sin^2(\theta) + \rho_1 cos^2(\theta))^2 \right]. \tag{15}$$

Intensity for circularly polarized light

The linear polarization dependence has been presented on multiple occasions.[2] Here, we also introduce the equivalent expression for circularly polarized incident light. The electric field for circularly polarization light can be expressed in terms of the Jones vector:

$$\mathbf{E} = |\mathbf{E}| Re\{|\psi\rangle exp[i(ky)]\}, \text{ where} \tag{16}$$

$$|\psi\rangle = \frac{1}{\sqrt{2}} \left[\begin{smallmatrix} 1 \\ \pm i \end{smallmatrix} \right] exp[i\alpha]\}. \tag{17}$$

The electric field can therefore be decomposed as $E_z(\omega) = \frac{1}{\sqrt{2}}|E(\omega)|$ and $E_x(\omega) = \frac{\pm i}{\sqrt{2}}|E(\omega)|$. For circularly polarized light, Eq. (8) can thus be expressed as:

$$\begin{bmatrix} P_x^{(2)}(2\omega) \\ P_y^{(2)}(2\omega) \\ P_z^{(2)}(2\omega) \end{bmatrix} = \epsilon_0 \begin{bmatrix} \frac{\pm i}{2}\chi_{xzx}|E(\omega)||E(\omega)| + \frac{\pm i}{2}\chi_{xzx}|E(\omega)||E(\omega)| \\ 0 \\ \frac{-1}{2}\chi_{zxx}|E(\omega)||E(\omega)| + \frac{1}{2}\chi_{zzz}|E(\omega)||E(\omega)| \end{bmatrix}, \text{ or} \tag{18}$$

$$\begin{bmatrix} P_x^{(2)}(2\omega) \\ P_y^{(2)}(2\omega) \\ P_z^{(2)}(2\omega) \end{bmatrix} = \frac{\epsilon_0}{2}|E(\omega)|^2 \begin{bmatrix} \pm i 2\chi_{xzx} \\ 0 \\ \chi_{zzz} - \chi_{zxx} \end{bmatrix}. \tag{19}$$

Using Eq. (19) in Eq. (4), we obtain an expression for the SHG intensity with circularly polarized incident light.

$$I_{SHG}^{Cir}(2\omega) = c\frac{\epsilon_0^2}{4}|E(\omega)|^4 \left[(4\chi_{xzx}^2 + (\chi_{zzz} - \chi_{zxx})^2 \right]. \tag{20}$$

Using the same notation as in Eq. (15), Eq. (20) can be written as:

$$I_{SHG}^{Cir}(2\omega) = c\frac{\epsilon_0^2}{4}\chi_{zxx}^2|E(\omega)|^4 \left[(4\rho_2^2 + (\rho_1 - 1)^2 \right]. \tag{21}$$

References

1 Butcher, P.N., and D. Cotter. 1990. The Elements of Nonlinear Optics. Cambridge University Press, London.

2 Plotnikov, S.V., A.C. Millard, ..., W.A. Mohler. 2006. Characterization of the myosin-based source for second-harmonic generation from muscle sarcomeres. *Biophys. J.* 90(2), 693–703.

3 Chen, W.L., T.H. Li, ..., C.Y. Dong. 2009. Second harmonic generation χ tensor microscopy for tissue imaging. *Appl. Phys. Lett.* 94(18), 2007–2010.

Gusachenko, I., G. Latour, ..., M.-C. Schannes-Klein. 2010. Polarization-resolved Second Harmonic microscopy in anisotropic thick tissues. *Opt. Express* 18(18), 19339–19352.